J. Fluid Mech. (1999), *vol.* 392, *pp.* 335–360. Printed in the United Kingdom

© 1999 Cambridge University Press

Boundary layer entrainment of sand-sized particles at high speed

By R. G. BATT, M. P. PETACH, S. A. PEABODY II AND R. R. BATT

TRW Space and Defense, Redondo Beach, CA 90278, USA

(Received 13 February 1998 and in revised form 5 March 1999)

An experimental study of entrainment of sand-sized particles in turbulent boundary layers has been performed in a high-speed wind tunnel at square-pulse flow speeds of 27 to 101 m s^{-1} and for soil bed lengths varying from 2.1 to 5.8 m. Because of high particle drag-to-weight ratios (D/W = 100–1000) and friction velocities (u_f) well above soil threshold friction velocities (u_{ft}; $10 \leqslant u_f/u_{ft} \leqslant 40$), the present results correspond to the suspension regime of dust lofting, in contrast to low-speed saltation flows ($1 \leqslant u_f/u_{ft} \leqslant 5$; $D/W \leqslant 15$). Results are obtained characterizing particle entrainment for both a natural soil (White Sands Missile Range (WSMR) sand; 50% finer-by-weight diameter, $\overline{D}_{50}$ = 180 μm) and a monosized sand sample (Ottawa sand, $\overline{D}_{50}$ = 250 μm). Measurements of local boundary layer velocities and dust densities were performed with traversing state-of-the-art diagnostics. Scouring rate data ($0.015 \leqslant \overline{m}_s \leqslant 0.30$ g cm^{-2} s^{-1}) and streamwise soil flux ($10 \leqslant Q \leqslant 150$ g cm^{-1} s^{-1}) as a function of bed length and velocity were determined.

Scouring rates were found to increase as the $\frac{3}{2}$-power of velocity, but decay as the inverse square root of dust bed length. Corresponding streamwise soil fluxes (also known as soil loss rates) increased to the $\frac{3}{2}$-power of velocity in contrast to the cube power dependence for low-speed results ($u_{free\text{-}stream} \leqslant 15$ m s^{-1}; $Q \leqslant 1.5$ g cm^{-1} s^{-1}). Comparison of scouring rate data (from pre/post-test soil loss measurements) with derived data based on the rate of change of streamwise flux with distance was favourable. WSMR rates were always lower than Ottawa sand rates, a result consistent with the lower repose angle for the Ottawa sand sample.

Both sets of soil data demonstrate that dust edges extend vertically to higher elevations than corresponding velocity edges. This result implies that the turbulent Schmidt number for the present flows is less than unity and of the order of 0.7. Favourable collapsing of the scouring rate data base was achieved when measured rates were normalized by the friction velocity mass flux, square root of edge Mach number and sand repose angle ratio. A universal rate of 0.3 ± 0.1 correlated well with the bulk of the data.

1. Introduction

As Denison & Hookham (1996) point out, interest exists in studying the high-speed soil sweep-up problem. Measured results on scouring rates are needed to support analytical studies of particle/debris sweep-up due not only to high-explosive detonations but also to such events as volcanic eruptions, tornadoes, air–ground disturbances from rotary and fixed-wing aircraft, mower/shredder operations, intense

dust storms, etc. The purpose of the current documentation is to summarize findings from a series of wind-tunnel experiments on soil scouring at high speed (Batt *et al.* 1993). Results as presented are intended to clarify boundary layer entrainment behaviour of sand-sized particles at high speed and to assist in modelling the soil sweep-up process in airblast hydrocodes (e.g. Hartenbaum 1971; Mirels 1984; Traci *et al.* 1987; Kuhl *et al.* 1990; Barthel 1990; Gaj & Small 1991 and Denison & Hookham 1996). Hartenbaum (1971) also conducted some soil scouring experiments with a monosized dust sample (Ottawa sand; $\overline{D}_{50} \approx 250\,\mu\text{m}$) at one bed length ($\approx 5.2\,\text{m}$) for free-stream flow speeds up to $118\,\text{m}\,\text{s}^{-1}$.

Pioneering and classical experiments on dusty boundary layer flow were performed by Bagnold (1941) in the late thirties. His work focused on the interplay between atmospheric winds and dry loose desert soils ($\approx 250\,\mu\text{m}$ particle sizes). As such his results correspond to low-speed flow conditions wherein free-stream velocities are $\leqslant 12\,\text{m}\,\text{s}^{-1}$ and to an equilibrium surface layer state known as saltation. The physical mechanisms controlling saltation are dominated by particle rebound/cratering effects coupled with gravity fallback phenomena. The saltation 'sand cloud' is in a dust-saturated (i.e. mass-limited) condition whose upper surface is clearly marked, does not grow with distance and is shallow in elevation extent as compared to the Earth's velocity boundary layer. Saltation flow thus corresponds to a moving dust layer wherein net scouring rates are zero.

Since Bagnold's experiments, numerous investigators have studied the physical mechanisms characterizing sand grain saltation. Important insight into the phenomenon has been provided by Owen (1964) who clarified the range of conditions under which saltation would occur. An extensive data base now exists on the saltation process both from wind-tunnel experiments and from full-scale field test measurements (e.g. Bagnold 1941; Chepil 1945; Gillette & Passi 1988; Shao, Raupach & Findlater 1993).

These background comments on saltation are given to highlight the distinction between the current dust sweep-up measurements at high speed (suspension regime per Owen 1964) and previous work. For example, results from the current wind-tunnel experiments correspond to growing turbulent boundary layers with sand flow rates increasing with distance, non-zero scouring rates and high-speed flow (wherein eddy currents are sufficiently large to suspend soil particles). Assuming an eddy velocity of the order of 10% of an imposed free-stream velocity and a particle size of $250\,\mu\text{m}$ (terminal velocity $\approx 1.0\,\text{m}\,\text{s}^{-1}$, Bagnold 1941) suspension is anticipated to begin setting in for boundary layer edge speeds greater than, say, $10\,\text{m}\,\text{s}^{-1}$. Clearly there exists a transition regime where progression from saltation to suspension flow takes place as a function of increasing velocity and decreasing particle size (Owen 1964). In the case of natural soils with wide particle size distributions, flow conditions exist wherein gravity forces become a factor in particle behaviour for large-diameter particles but less important for soil fines.

The current experiments were performed in a special purpose wind tunnel, the Dust Sweep-Up (DSU) Wind Tunnel. Measurements were conducted with state-of-the-art diagnostics at flow speeds as high as $101\,\text{m}\,\text{s}^{-1}$ and for soil beds up to 5.8 m in length. Data are presented characterizing soil scouring rates and profile behaviour as a function of soil type (dry/erodible soils only), free-stream velocity and bed length.

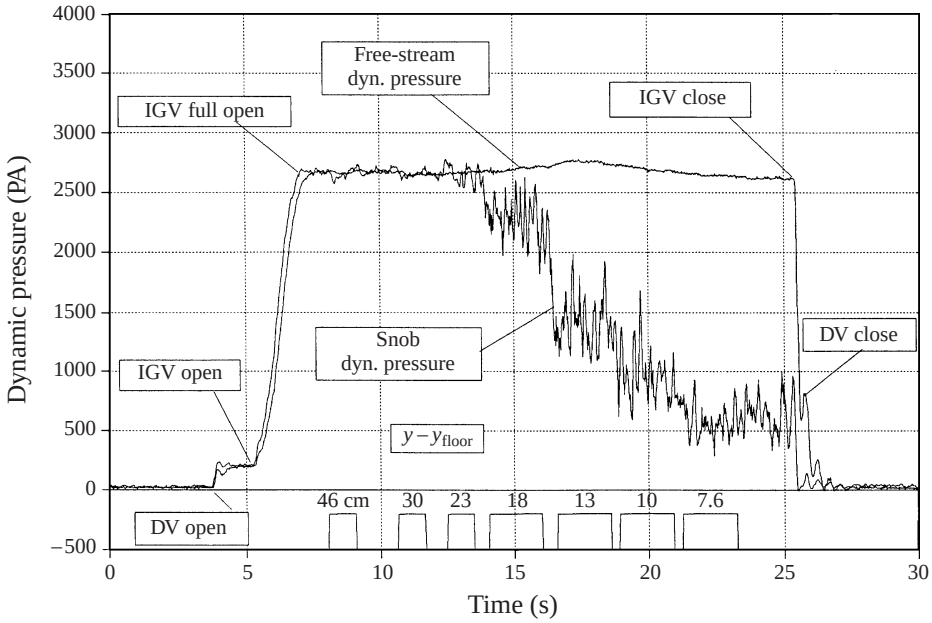

FIGURE 1. Typical time history trace for dynamic pressure data from the traversing Snob probe (WSMR soil bed; free-stream, i.e. boundary layer edge, velocity = 66.5 m s^{-1}; bed length = 2 m; DSU43).

2. Experimental technique

2.1. *Wind tunnel*

The DSU wind tunnel is of open-loop type (contraction ratio 6.85) with air supplied by a Buffalo Forge centrifugal fan. It is designed to support dusty flow experiments up to a Mach number $\leqslant 0.3$ by use of engine speed control (800–1800 RPM) and/or damper/guide vane adjustments. Both vane sets are remotely controlled by fast-response actuators to provide sharp turn on/off flow conditions ('square-pulse' free-stream flow environment). A large-capacity louvered dust separator controls the facility's outlet flow and removes dust particulates from the exhaust gases.

The wind tunnel's test section has an overall length of 7.3 m and an inlet cross-section of 0.46 m width $\times$ 0.71 m height. Multiple access ports (0.91 m $\times$ 0.31 m; sides, bottom and top) are included to accommodate flexibility in instrumentation setup and to aid in soil installation/maintenance.

The measurements reported herein provide data obtained with both facility monitoring instrumentation and diagnostics mounted on two vertically traversing probe/detector mounting struts. One mounting strut, the interior probe strut, was used as a support structure for local, i.e. *in situ*, measurements of air/dust velocity probes. An X-ray dust density detector system was mounted separately on a yoke-type external structure with the X-ray tube installed on one arm of the yoke and the photodiode/scintillator detector on the other arm. The two traversing struts were synchronized to move their respective diagnostics simultaneously and in a co-located manner. Computer-controlled rapid start/stop motors were used to power and to position each traverse system according to pre-set vertical location/time requirements.

A plot of signal output from a dusty Pitot-static probe for a typical DSU run (DSU 43) is given in figure 1. The trace shown illustrates a nominal output response from a

dusty boundary layer traverse for the Snob probe as it is moved in a stop-hold-move fashion from the free-stream core flow (0.46 m above the wind tunnel's steel floor) towards the dust bed. For this run, the probe measurement station (station 3) was located 4.67 m from the test section entrance. The initial dust bed thickness was 5.1 cm and the bed's leading edge was positioned 2 m upstream of the probe traverse location.

The DSU43 trace of figure 1 illustrates the typical flow turn on/off sequence for the DSU experiments and the square pulse nature of the free-stream flow. Note the use of damper vanes (DV, located upstream of the blower) and inlet guide vanes (IGV, radial vanes mounted in the blower's inlet cone). Annotations on figure 1 further illustrate the relative sequence and facility flow response for the different test event times noted.

Shown also on figure 1 is a probe-position/data-acquisition signal plot. The plateau duration for each 'top hat' position signal represents the time increment at which the probe was stationary at the elevation values cited (probe elevation above steel floor). The times between top hats represent a moving traverse condition. For each run, the traverse started at its preset 'home' or maximum position, then was stepped down to its lowest elevation.

In figure 1 not only do the Snob core flow results compare favourably with the tunnel's free-stream Pitot-static pressures, but Snob post-test baseline pressures are in good agreement with pre-test levels. Note that some variations in tunnel free-stream velocities (dynamic pressures) occur during the run duration for a given experiment. However, such variations are corrected for in reduced velocity results in that all DSU velocity profile data have been normalized by the temporally correct free-stream condition corresponding to each data point.

2.2. *Soil bed samples*

The soil materials tested (particle specific gravity ≈ 2.6) include a monosized rough sphere sample (Ottawa sand; $\overline{D}_{50} \approx 250\,\mu\text{m}$; $1.62\,\text{g cm}^{-3}$) and a natural soil (WSMR sand, $1.38\,\text{g cm}^{-3}$) with a wide particle size distribution. The WSMR samples were sieved (#20) to a 50% finer-by-weight diameter ($\overline{D}_{50}$, i.e. that diameter for which the weight of all particles of less diameter corresponds to one-half the sample weight) of 180 μm ($\overline{D}_{100} \approx 800\,\mu\text{m}$; $\overline{D}_{10} \approx 60\,\mu\text{m}$).

For the DSU experiments, typically 5.1 to 7.6 cm of soil material was laid out on the tunnel's test section floor extending forward of the measurement station to accommodate the selected bed length of interest. The bed was terminated approximately 1 m downstream of the probe location to avoid forward feeding of bed/floor discontinuity disturbances. Each pre-test bed was installed by pouring bags of soil material through the tunnel side port openings and then scraping the top surface of the bed to the desired bed height with template guides. All tests were run with dry loose (erodible) soils (moisture content $\leqslant 2\%$). Also all results correspond to pre-bed boundary layers established over a floor surface roughened using sandpaper (#100 grit) and/or Astroturf matting bonded to the tunnel's floor. In order to mitigate dust/flow disturbances at bed leading edges all tests were run with a thick upstream boundary layer, smooth surface changes (minimal discontinuities which could generate downstream running vortices) and a shallow ramp angle ($\approx 10^\circ$) to the bed leading edge (to attenuate edge erosion phenomena such as snow-plough and/or dunning effects).

Average scouring rate data presented herein are based on pre/post-test spanwise-averaged bed heights. Some erosion of bed leading edges occurred for all experiments. Such bed length decreases were of the order of 15 cm (for the low-speed runs) to 60 cm

(for the high-speed test cases), varied linearly with time and have been accounted for herein in an approximate manner by referencing results to a time-averaged leading-edge distance. Close-up photographs, PSD data and pre/post test bed layout details for both dust samples and for all test runs are presented in Batt *et al.* (1993).

2.3. *Flow diagnostics*

Of the wide selection of instrumentation considered for the DSU experiments, results presented and analysed herein were developed from essentially four measurement techniques: a dusty-gas Pitot-static probe (TRW's Snob probe; Batt, Petach & Peabody 1995); an X-ray dust density detector (Batt *et al.* 1993); a dust capture tube rake; and pre/post-test mass-loss/surface-recession measurements. This latter diagnostic approach characterized soil scouring rates by use of surface recession data (pre/post bed height measurements) and/or soil mass loss results (pre/post-test soil weighing). Both these measurement procedures made use of the square-pulse nature of the DSU tunnel's free-stream flow to determine scouring rates by averaging weight loss per unit area over the flow pulse time duration. Results obtained from this approach demonstrated that so-determined scouring rates based on either surface recession data or mass loss measurements compared favourably.

2.4. *Snob probe*

This dust-velocity probe operates like a typical Pitot-static pressure probe but is hardened and configured to respond to local air pressures and to be relatively insensitive to particle loading phenomena. The vented probe design was developed in support of diagnostics development for airblast field test experiments. It incorporates three transducers in a single probe body to measure static, total and total/static differential pressures. This tri-sensor approach not only provides redundancy in measurement but also gives direct readouts of air-only dynamic pressures. The vented nozzle design (throat contraction 6.25) also allows long-duration testing without cavity plugging while measuring pressures to within 1% accuracy. For the Snob results presented herein, essentially local air velocity data derived from dynamic pressure measurements, the probe was vented to the downstream tunnel flow at the base of the probe strut.

For all experiments the Snob probe was paired in a co-located manner with a dusty-gas total-pressure probe, often designated a Greg probe (Batt *et al.* 1993). This probe, because of its force plate design, measures the full effects of the gas stagnation pressure and the local dust momentum flux. Even though Snob/Greg data were measured for all DSU experiments, reduced results herein have been limited to Snob velocity results only. A complete set of raw Greg data is available on archival tapes, however, and can be processed if warranted.

2.5. *X-ray dust density detector*

The X-ray detector diagnostic is a modification of the line-of-sight X-ray attenuation system that has been operated in previous shock tube experiments. The system consists of an X-ray source on one side of the wind tunnel and an X-ray detector on the other side. The attenuation of the X-ray beam (6° included-angle-cone) is a function of the mass density of the dust in the X-ray beam path.

The X-ray source and detector are mounted on a movable yoke so that they can be raised or lowered to obtain dust density measurements at various heights. The yoke is moved up and/or down on a traverse system by a stepper motor under computer control and is synchronized with the stepper motor that controls the Snob traverse

system. This allows the X-ray beam to remain positioned at the same elevation as the Snob probe during a run. The X-ray beam passes through the wind tunnel approximately 2 cm upstream of the tip of the Snob gauge to provide dust density measurements co-located with the Snob data. The wind-tunnel ports at the X-ray location had vertical slots cut into them to act as windows. The windows were covered by 0.25 mm thick mylar which was mounted flush to the inside surface of the wind tunnel by a gel-type cyanoacrylic glue. *In situ* calibration of the X-ray detector signal was performed for each run using mounted areal density target samples. Additional details for the X-ray dust density measurement technique are provided in Batt *et al.* (1993).

2.6. *Dust capture tube rake*

Collected mass data from dust capture tubes at multiple elevations for the DSU boundary layer experiments have been obtained for all of the DSU test cases. Mass flux profiles have been prepared by normalizing the collected mass data by tube frontal area and test pulse duration time.

The five-tube dust capture rake (J. E. Cockayne, Science Applications Intl. Corp.) was installed in the DSU wind tunnel 12 cm from the tunnel's centreline. The tubes were sized to provide adequate capture efficiency in collecting the largest particles for the WSMR dust samples ($\approx$ 1 mm). Each tube was made from 1.27 cm OD stainless steel tubing (1.09 cm ID) and individually swedge-locked into the tunnel's steel floor to allow independent setting of inlet elevation. Leading edges for all five tubes were sharpened to 10° half-angle edges. Tube axial lengths varied from 11.4 cm to 24.1 cm corresponding to stem diameter distances of 9 and 19, respectively. Stem-induced disturbances and tip oscillation effects due to excessive tube length were therefore small. Results discussed herein were obtained by the direct vacuum technique wherein each tube's under-floor outlet was connected to an individual suction pump and samples collected in fine woven vacuum bags.

3. Results and discussion

Over the course of the DSU programme, a total of 64 tests were conducted, a number of which were carried out to evaluate tunnel/diagnostic performance and test set-up considerations. Results described here were obtained with some selected DSU experiments, listed in the abbreviated test matrix of table 1.

3.1. *Boundary layer profiles*

Typical boundary layer profiles from the current study for velocity, dust density and mass flux are shown in figures 2, 3 and 4, respectively. The results correspond to WSMR data for a nominal free-stream velocity (i.e. the boundary layer edge velocity, u_e) of 97.5 m s^{-1} and were obtained by time-averaging (for a given fixed probe position) the Snob and X-ray measurements as a function of elevation (y) above the soil bed. Because surface recession occurred at a linear rate (as a result of the square-pulse nature of the free-stream flow and as confirmed by a surface recession detector (M. D. Cousins, Stanford Research Institute)), probe/surface elevation data were determined from post-test analysis of bed depth profile data and probe position settings.

To evaluate the extent of flow similarity, approximate curve fits to profiles of velocity (u) and dust loading factor ($k \equiv \rho_d/\rho_e$, where ρ_d and ρ_e correspond to the dust and air densities, respectively) are also indicated on figures 2 and 3. For the

Dust type	DSU test	Free-stream (edge) velocity ($m\,s^{-1}$)	Bed length (m)	Test time (s)
WSMR	44	27.1	2.16	21
	49	36.9	3.86	21
	51	32.3	5.79	22
	43	66.5	2.01	19
	46	67.4	3.81	21
	50	60.7	5.66	21
	45	99.4	2.16	22
	48	101.5	3.91	23
	52	94.8	5.79	21
Ottawa	60	32.9	2.13	20
	57	32.9	4.09	21
	54	32.9	5.72	22
	59	64.3	1.93	21
	56	68.6	3.76	22
	53	69.2	5.59	22
	61	95.1	2.13	20
	58	96.3	3.89	19
	55	99.4	5.74	19

TABLE 1. Dust sweep-up test matrix.

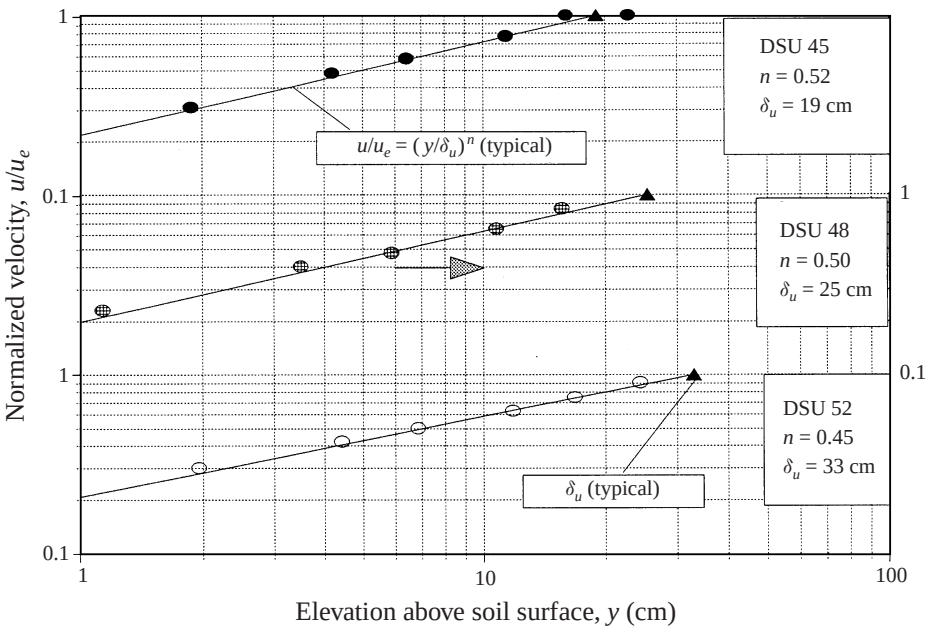

FIGURE 2. Typical profiles of boundary layer velocity (u) as normalized by boundary layer edge velocity (u_e): WSMR soil bed ($u_{free\text{-}stream} \equiv u_e \approx 98.6\,m\,s^{-1}$). u_e and bed length data are given in table 1.

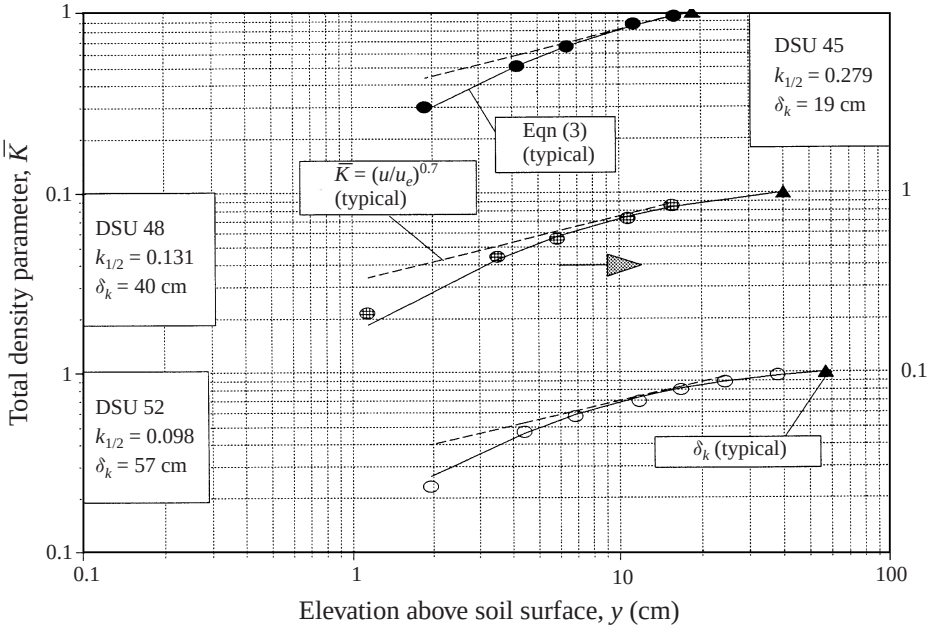

FIGURE 3. Typical profiles of total density parameter ($\overline{K} = (1 + \rho_d/\rho_e)^{-1}$): WSMR soil bed ($u_{free\text{-}stream} \equiv u_e \approx 98.6\,\mathrm{m\,s^{-1}}$). Velocity and bed length data are given in table 1.

velocity results, a power-law model is used to correlate the data, namely

$$u/u_e = (y/\delta_u)^n, \tag{1}$$

where δ_u represents the tangent-slope velocity thickness in log-log coordinates and n is the power-law exponent. This two-parameter fit is seen to be in good agreement with the figure 2 results.

In figure 3 the dust density profiles are plotted in terms of total density data ($\overline{K}$; Denison & Baum 1986), i.e.

$$\overline{K} = (1 + k)^{-1}, \tag{2}$$

with $\overline{K}$ approaching unity at the boundary layer's edge and zero near the soil surface. The curve fits noted on figure 3 also use a two-parameter definition but based on a near-surface inverse linear decay law for k, namely

$$k = k_{1/2}[(y/\delta_d)^{-1} - 1]. \tag{3}$$

Here $k_{1/2}$ corresponds to the loading factor magnitude at the 50% profile thickness point ($y/\delta_d = 0.5$) and δ_d represents the dust edge thickness. Both parameters are determined by a two-point matching of the dust density profile shape. In general, overall WSMR and Ottawa sand results for $\overline{K}$ are in good agreement with the curve fit formulation shown.

The two sets of mass flux data in figure 4 illustrate the comparison between results based on velocity/dust density profile data and as obtained by dust capture-tube measurements. The data are seen to compare favourably, providing a redundancy check on measurement consistency. Additional profile plots similar to figures 2–4 are available in Batt *et al.* (1993) for all DSU run cases.

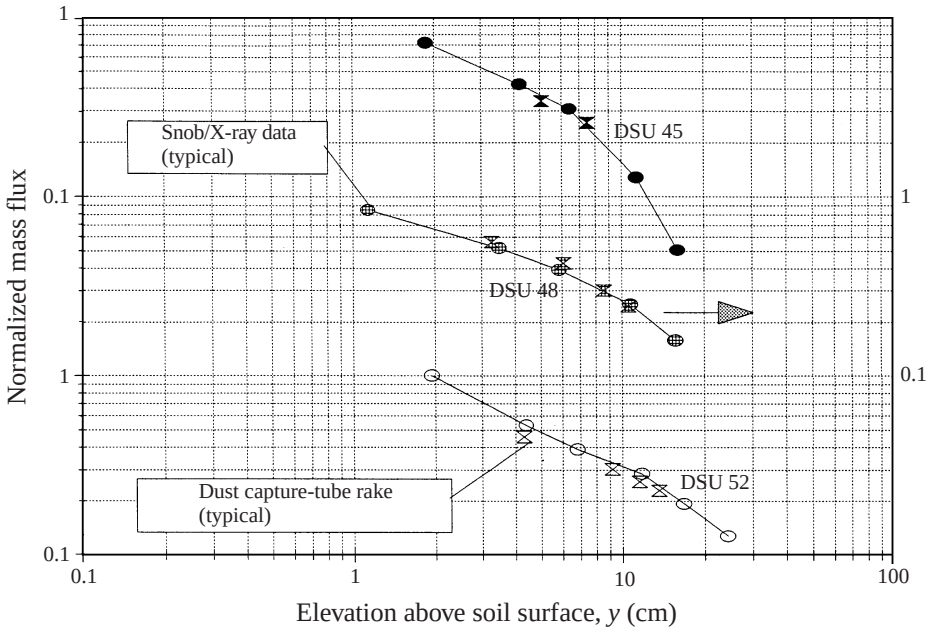

FIGURE 4. Typical profiles of boundary layer dust mass flux, $(\rho u)_d$, as normalized by edge mass flux, $(\rho u)_e$: WSMR soil bed ($u_{free\text{-}stream} \equiv u_e \approx 98.6\,\mathrm{m\,s^{-1}}$). Velocity and bed length data are given in table 1.

3.2. *Edge thickness distributions*

Summarized edge thickness data (δ) from the current series of experiments are shown in figures 5 and 6, illustrating the dependence of boundary layer thickness on bed length and free-stream velocity, respectively. Both sets of soil data demonstrate that dust edges (δ_d) extend vertically to higher elevations than corresponding velocity edges (δ_u). This finding is consistent with Greg probe measurements (air *plus* dust pressures) which show that dusty-gas motion exists at high elevations where Snob measurements read, essentially, the free stream. The importance of this result, which also is observed in turbulent shear flows when comparing scalar and velocity edges, is that a turbulent Schmidt number less than unity is appropriate in flow modelling analyses.

Note that, for both soil samples, velocity boundary layer growth correlates approximately with square root of distance (figure 5). Such a thickness variation with axial *distance* is comparable to boundary layer growth for laminar ($\delta_u \sim x^{1/2}$) and turbulent ($\delta_u \sim x^{4/5}$) boundary layer flows. However, the edge thickness dependence on *velocity* evidenced in figure 6 for the two soil samples, given approximately by ($\delta_u \sim u_e^{1/2}$), is at odds with the decay behaviour for established boundary layer flows ($\delta_{u,lam} \sim u_e^{-1/2}$ and $\delta_{u,turb} \sim u_e^{-1/5}$). The current thickness-enhancement-with-velocity result, however, is considered a reflection of the interaction between the boundary layer decay process associated with increased flow Reynolds numbers (due to velocity increases and particle loading effects) and boundary layer thickening induced by mass addition increases. This explanation for the observed velocity dependence is consistent with results for the blowing boundary layer problem (e.g. Schlichting 1955; Mirels 1984) which also involves the counteracting effects of reduction in thickness, due to Reynolds number increases, and growth enhancement for those cases where wall

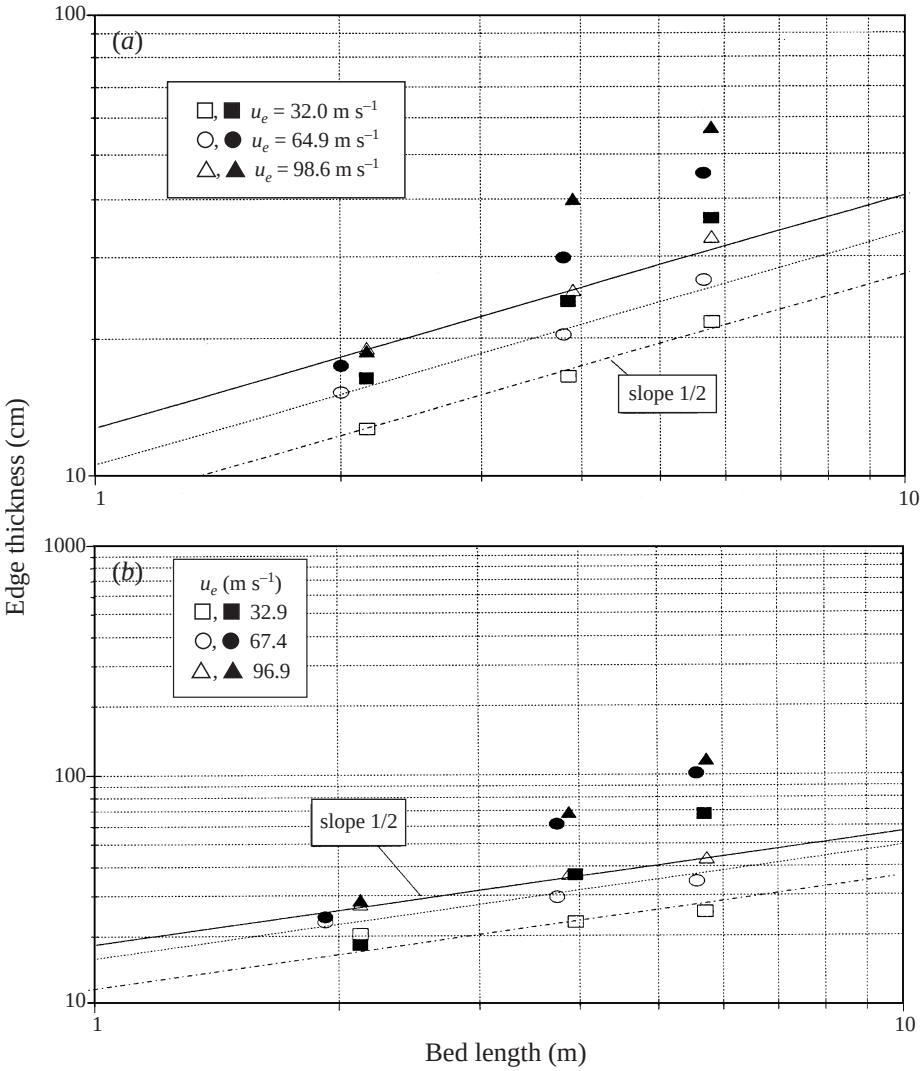

FIGURE 5. Variation of velocity (δ_u, open symbols) and dust density (δ_d, closed symbols) edge thickness with bed length for (*a*) WSMR and (*b*) Ottawa sand soil beds and three boundary layer edge velocities (u_e).

injection increases with flow velocity. Note that Hartenbaum (1971) also measured a velocity dependence for boundary layer edge growth ($\delta_u \sim u_e^{3/8} - u_e^{1/2}$) comparable to results herein for his experiments with Ottawa sand under similar test conditions.

Finally note that Ottawa sand thickness, for both velocity and dust density, are substantially larger than corresponding WSMR data. Such a result is one of several relevant differences in particle entrainment behaviour between monosized Ottawa sand soil and the WSMR natural sand sample.

3.3. *Velocity profile scaling*

Normalized velocity data (u/u_e) for both WSMR and Ottawa sand samples are summarized in figure 7 versus elevation above the soil surface (y) as normalized by the velocity edge thickness (δ_u). The velocity curve fit of equation (1) is also provided

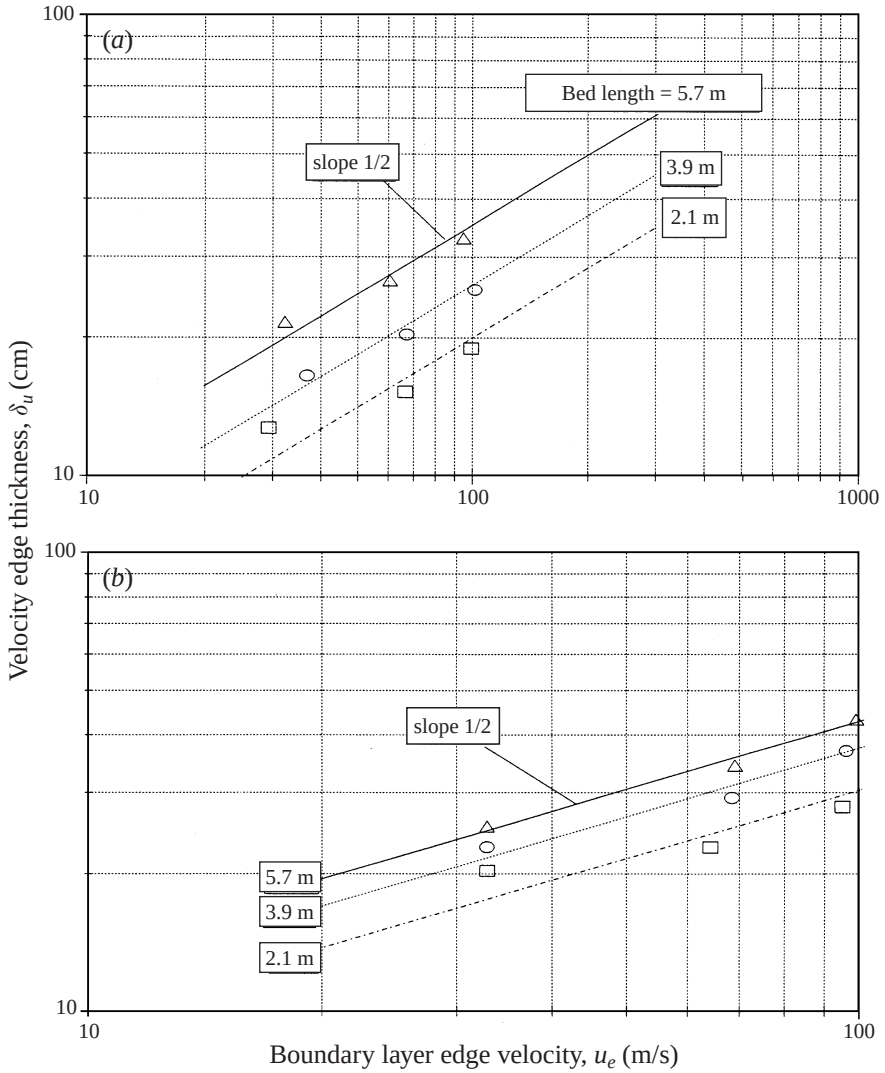

FIGURE 6. Variation of velocity edge thickness (δ_u) with boundary layer edge velocity (u_e) for three bed lengths, (*a*) WSMR; (*b*) Ottawa sand soil beds.

on figures 7(*a*) and 7(*b*). Results as shown, in general, confirm the self-similar nature of the velocity profiles. Values for the power-law exponent (n) for the WSMR and Ottawa sand data are 0.5 ± 0.05 and 0.65 ± 0.1, respectively.

In addition to evaluating profile similarity of the DSU velocity data by the curve-fitting procedure shown, velocity results have also been plotted in semi-log format (Batt & Peabody 1995) to test the flow's 'law-of-the-wall' velocity behaviour, namely

$$u = (u_f/\overline{k}) \ln (y/y_0) + u_0. \tag{4}$$

Here u_f and u_0 represent the friction and reference velocities, respectively, $\overline{k}$ corresponds to the von Kármán constant and y_0 is the effective wall roughness height (as determined from the coalescence point of multiple velocity profiles). When velocity data are plotted in the conventional semi-log format, equation (4) illustrates that the

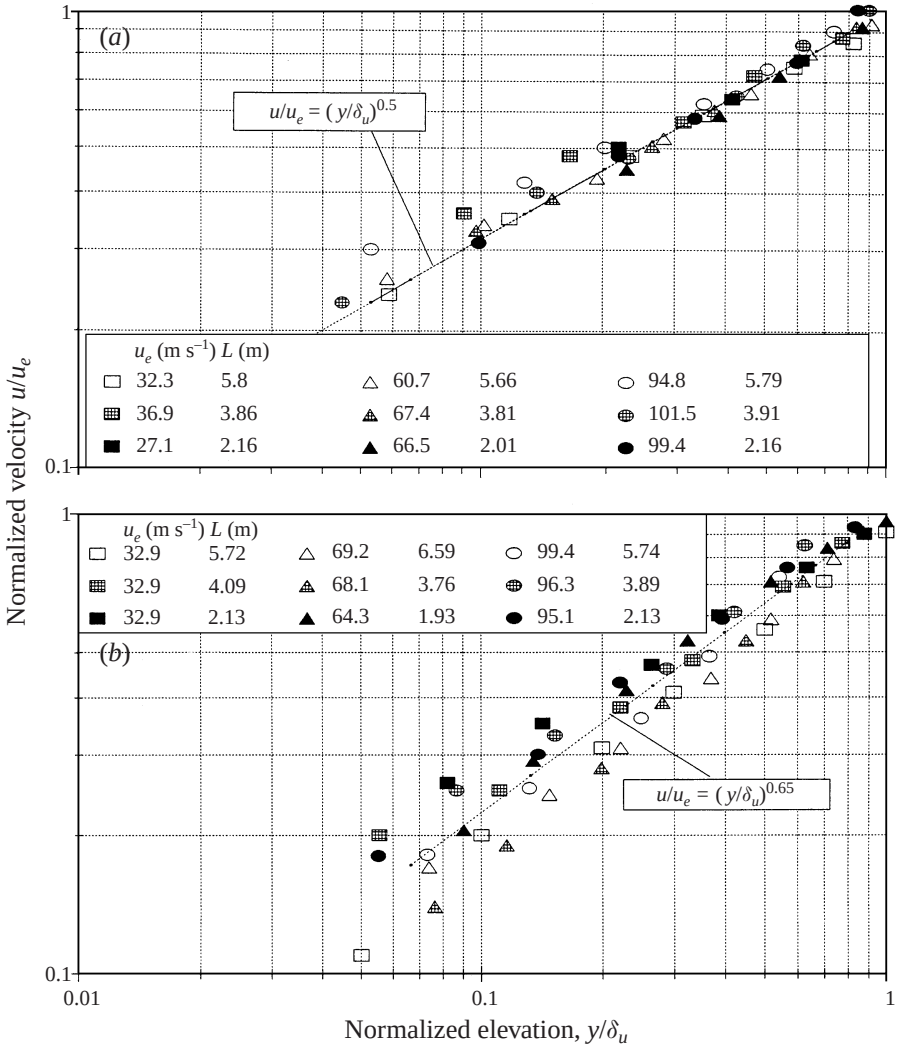

FIGURE 7. Similarity scaling of profiles of normalized velocity (u/u_e) as a function of normalized elevation (y/δ_u) for (*a*) WSMR and (*b*) Ottawa sand soil beds and for three boundary layer edge velocities (u_e) and three bed lengths (L).

near-surface slope of the velocity data corresponds to the friction velocity for a fixed free-stream flow condition. It is estimated that, because of curve-fitting limitations and surface elevation uncertainties, so-determined values for u_f can be measured to within an accuracy of $\pm$15%. Velocity profile data for three different free-stream velocities at a given bed length distance were found to agree with equation (4) when results were co-plotted to determine a test-case reference velocity and focus height. A plot of the data in normalized coordinates is presented in figure 8 and the low elevation results are seen to collapse to a common law of the wall scaling. Such a result supports the dusty law-of-the-wall modelling approach put forward by Denison & Baum (1986) and others for treating the dusty boundary layer problem. The rough wall correlation given by equation (4) is also shown in figure 8.

Reduced friction velocities for the current results are summarized in figure 9. For a

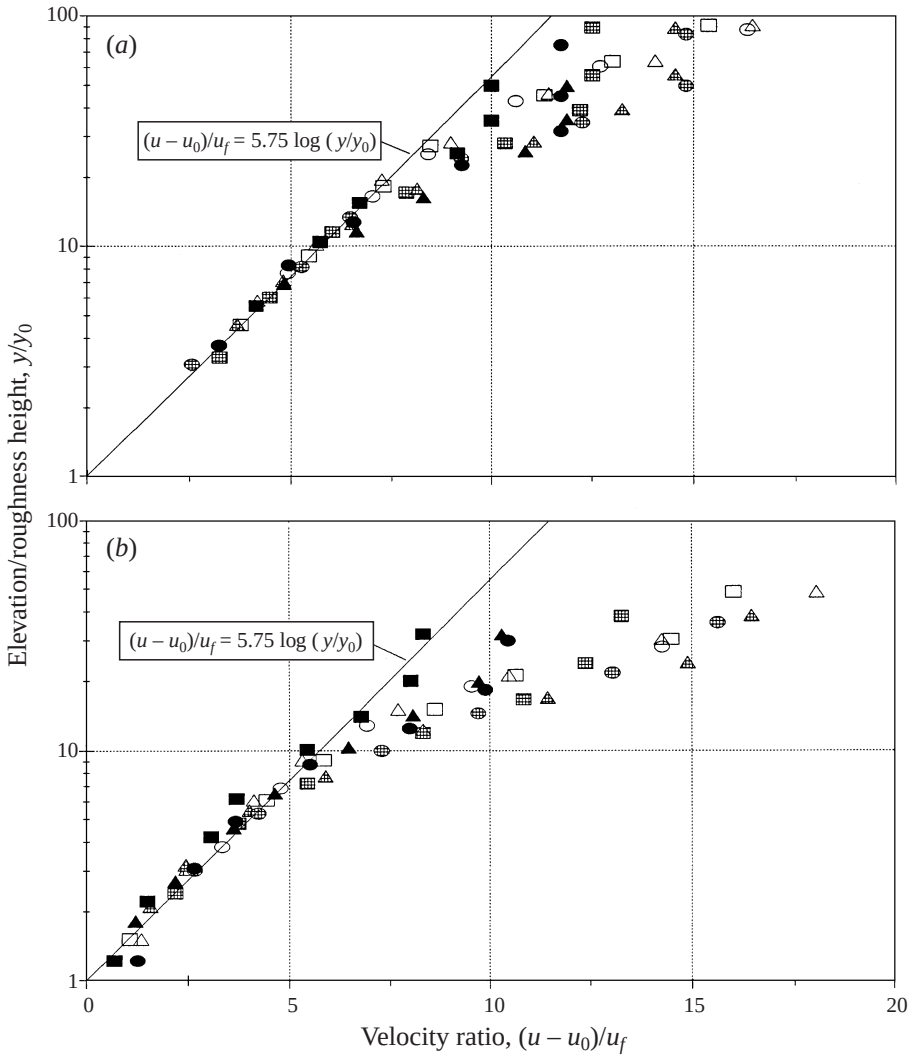

FIGURE 8. Summary of velocity profiles in semi-log format of law-of-the-wall scaling for (*a*) WSMR and (*b*) Ottawa sand soil beds and for three boundary layer edge velocities (u_e) and three bed lengths. Symbols same as figure 7.

given bed length, the data indicate a near linear variation of u_f with the edge velocity (u_e) with the ratio u_e/u_f increasing from ≈ 12 at the 2.1 m station to ≈ 17 for the longer bed lengths. Since the surface friction coefficient (c_f) is related to the velocity ratio by

$$c_f/2 = (u_f/u_e)^2, \tag{5}$$

the observed trend in u_e/u_f with bed length is consistent with the corresponding and expected reduction in c_f with distance. A replotting of the u_f data in figure 10 illustrates that friction velocity decays with bed length as approximately the inverse square root of distance. This finding will be shown to be in agreement with dust scouring reduction with distance as measured herein. Note also that the present friction velocities are substantially larger than terminal velocities ($u_{terminal} \approx 1\,\mathrm{m\,s^{-1}}$; Bagnold 1941) such that the Bagnold criterion for the onset of particle suspension,

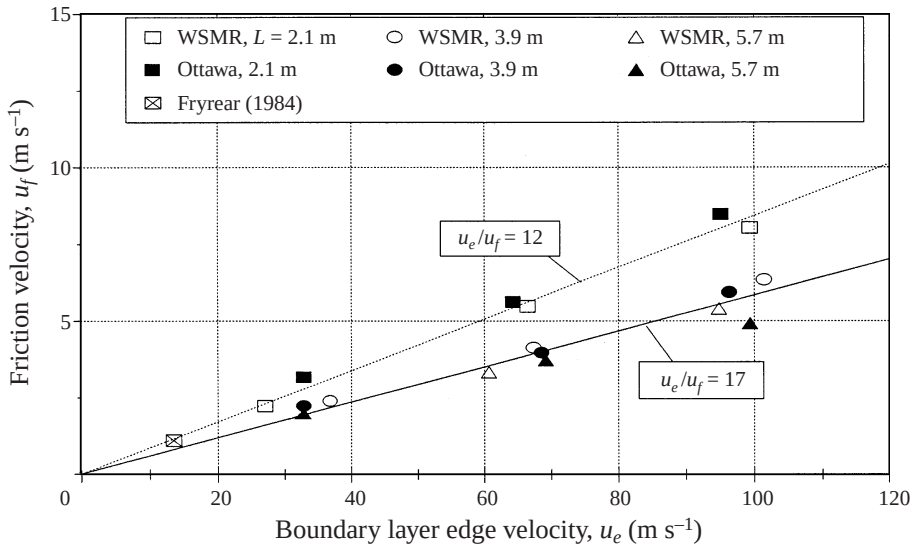

FIGURE 9. Variation of friction velocity (u_f) with boundary layer edge velocity (u_e) for WSMR and Ottawa sand soil beds for three bed lengths (L).

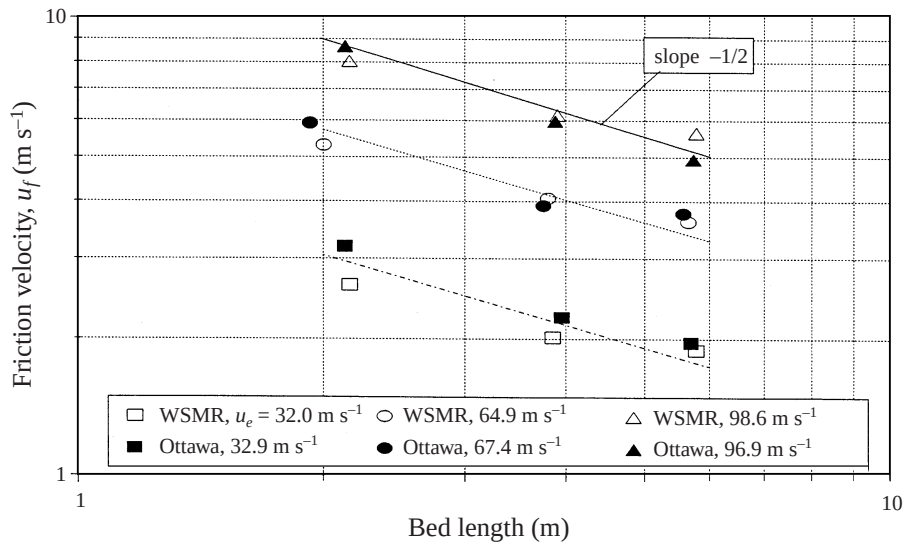

FIGURE 10. Variation of friction velocity (u_f) with bed length for WSMR and Ottawa sand soil beds for three boundary layer edge velocities (u_e).

namely

$$7u_f > u_{terminal}, \tag{6}$$

is readily satisfied. In addition, measured friction velocities are also considerably larger than threshold friction velocities ($u_{ft} \approx 0.2\,\mathrm{m\,s^{-1}}$; Bagnold 1941) for the soils tested, namely

$$10 \leqslant u_f/u_{ft} \leqslant 40. \tag{7}$$

As Owen (1964) points out, this range of friction velocity implies, like the Bagnold criterion, that results herein for both the WSMR and Ottawa sand soils correspond to

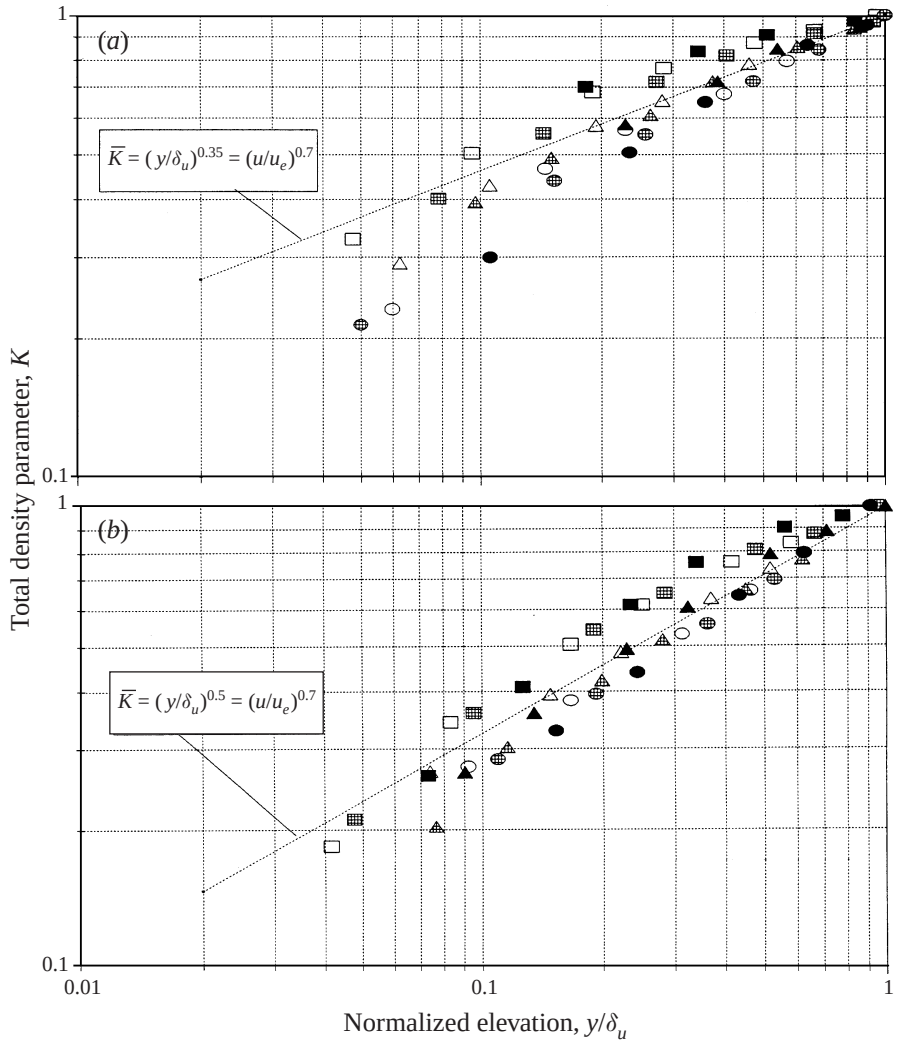

FIGURE 11. Similarity scaling of profiles of total density parameter ($\overline{K} = (1+\rho_d/\rho_e)^{-1}$) as a function of normalized elevation (y/δ_u) for (*a*) WSMR and (*b*) Ottawa sand soil beds and for three boundary layer edge velocities (u_e) and three bed lengths (L). Symbols same as figure 7.

the suspension regime for particle motion, in contrast to saltation-type flow common to low-speed test conditions.

3.4. *Dust density profile scaling*

Summarized dust density profile results ($\overline{K}$) for the DSU experiments are presented in figure 11. Co-plotted on figure 11 are data fits for ($\overline{K}$) based on scaling velocity profiles to dust density profiles through use of the turbulent Schmidt number (Sc) approximation (per Denison & Baum 1986), namely

$$\overline{K} = (u/u_e)^{Sc}. \tag{8}$$

Because the dust particle layer grows at a faster rate than the velocity (namely $\delta_d \sim x$ in contrast to $\delta_u \sim x^{1/2}$), this correlation approach, which in effect stretches velocity profiles to match the lateral extent of the dust density data, is seen to be in fair

agreement with the bulk of the data when an Sc value of 0.7 is used. Note that the dotted curves in figure 11 represent velocity data adjusted for Schmidt number effects (i.e. for example, the curve labelled $\overline{K} \approx (y/\delta_u)^{0.5}$ in figure 11*b* should be recognized as corresponding to $\overline{K} = (u/u_e)^{0.7}$).

3.5. *Scouring rate scaling*

For the DSU programme, local scouring rates ($\overline{m}_s$) were measured with three independent techniques: surface recession $\overline{m}_s$ (by pre/post-test bed depth profile measurements); mass loss scouring rate (by pre/post-test soil weighing procedures); and an $\overline{m}_s$ based on the gradient with distance of streamwise soil flux (Q). Here Q corresponds to the total soil mass flow rate per unit width moving past a given axial station. It is determined in the conventional manner by integrating the dust flux profiles ($\rho_d u$, where it can be shown for the current flow speeds and small particles that the particle velocities (u_d) and air velocities (u) are approximately equal) across the vertical extent of the boundary layer (δ), i.e.

$$Q = \int_0^{\delta} (\rho_d u) \mathrm{d}y. \tag{9}$$

In the case of profile similarity, Q can also be represented approximately as

$$Q \approx \rho_e u_e \delta \int_0^1 (\rho_d u / \rho_e u_e)\, \mathrm{d}(y/\delta). \tag{10}$$

The first two methods for measuring local scouring rate, which make use of the tunnel's square-plus free-stream flow (figure 1), compared favourably during early checkout testing. Because of this good agreement, most $\overline{m}_s$ measurements for the DSU tests reported herein have been based on the depth profile technique.

The third $\overline{m}_s$ measurement procedure, the rate of change of Q with distance, namely

$$\mathrm{d}Q/\mathrm{d}x \equiv \overline{m}_s, \tag{11}$$

provides a consistency check on overall DSU results. It is based on interrogating the soil mass flux behaviour past a given station and determining the local net increase of soil loss rate caused by soil scouring at the surface.

For DSU, Q data for three axial locations were determined for each of three free-stream velocities and results are presented in figure 12. The data exhibit a square-root dependence on bed length and empirical curve fits for each test velocity of the form

$$Q = c_1 x^{0.5} + c_2 \tag{12}$$

are provided therein. Although only three data points are used in the curve fits shown, the differentiated version (equation (11)) of the correlation curve becomes an important independent measure of soil scouring rate, as to be discussed shortly. Note that the observed square-root behaviour is also consistent with the relationship for Q given by equation (8) since the boundary layer profiles are approximately self-similar (figures 7 and 11) and the layer thickness grows to the half-power of bed length (figure 5).

Corresponding derived scouring rates based on equations (11) and (12) are shown as the curves in figures 13(*a*) and 13(*b*) where the rate data are plotted as normalized by the boundary-layer-edge mass flux ($\rho_e u_e$), i.e. $\overline{m}_s/\rho_e u_e$. Comparison in the figures of measured rates (from pre/post-test measurements of spanwise-averaged surface heights) with results from the differentiated curve fits of figure 12 is seen to be favourable both quantitatively and in terms of data trends. As to be expected from

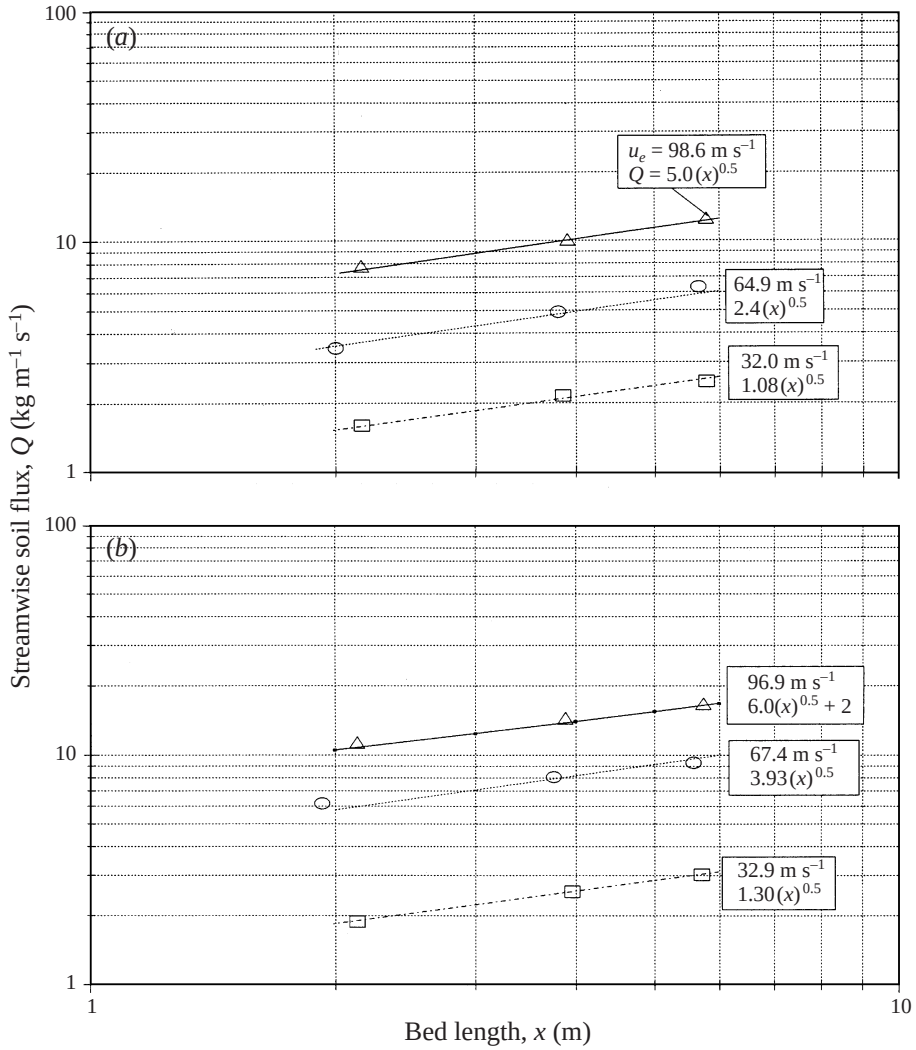

FIGURE 12. Variation of streamwise soil flux (Q) with bed length for (*a*) WSMR and (*b*) Ottawa sand soil beds for three boundary layer edge velocities (u_e).

the streamwise flux data of figure 12 (equation (12)) and the relationship between soil loss rate and scouring rate (equation (11)), the scouring rates decay approximately with bed length as the inverse square root of distance, namely

$$\overline{m}_s = 0.5 c_1 x^{-0.5}. \tag{13}$$

A replotting of the DSU scouring rate data as a function of free-stream velocity is given in figure 14(*a*). Each of the results for the two soils tested indicates that normalized scouring rates ($\overline{m}_s/\rho_e u_e$) increase, approximately, as the half-power of velocity (i.e. $\overline{m}_s \sim u_e^{3/2}$). For comparable experimental test conditions Hartenbaum (1971) and Mirels (1984) predict $\overline{m}_s \sim u_e^{9/8} - u_e^{5/4}$. As expected from the thickness data of figure 5, Ottawa sand erosion rates are larger than corresponding WSMR results.

Note that soil scouring experiments in Batt *et al.* (1993) suggested that soil friction angle (and/or repose angle, α) represented an approximate correlator (measure) of

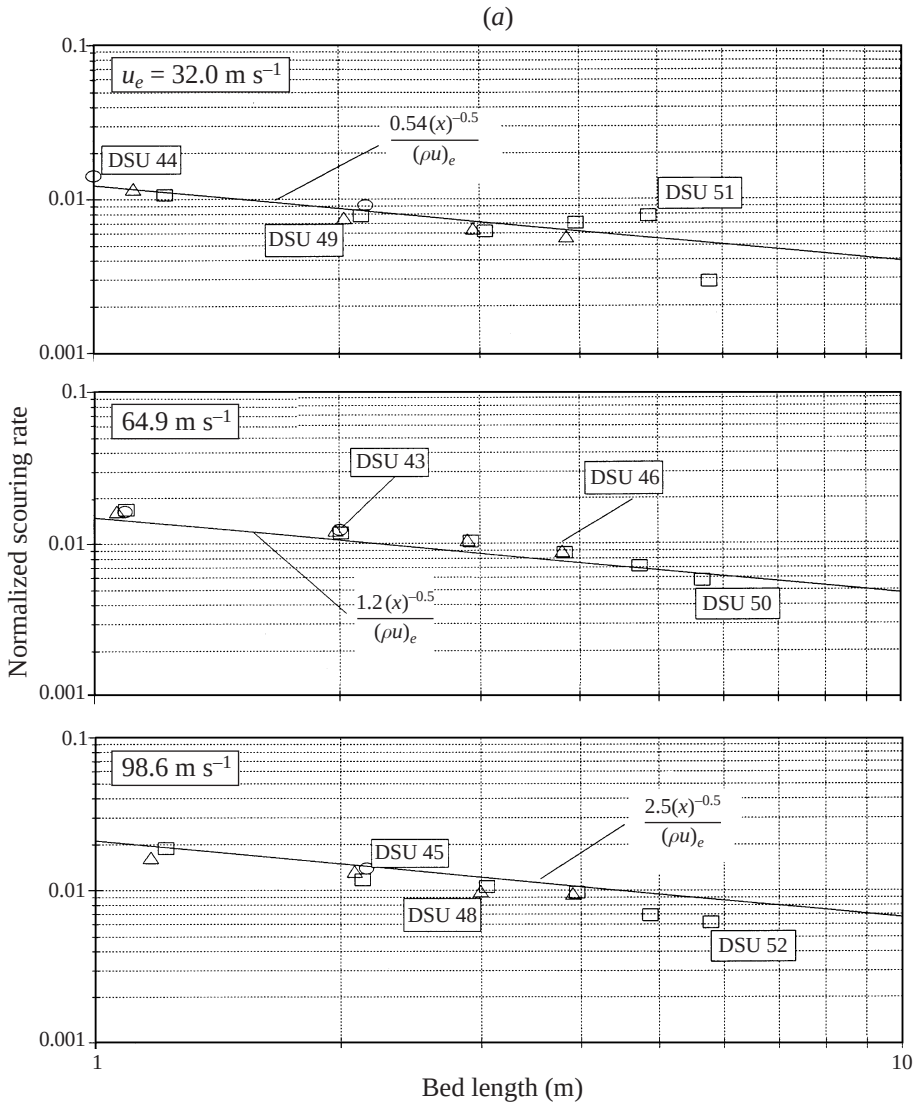

FIGURE 13 For caption see facing page.

a soil's scouring potential. Such a soil characterizing parameter, which reflects the geometry of the sand grains and their interlocking frictional behaviour, indirectly relates to their ability to become suspended in response to local shear forces. It was found that soils with low friction (repose) angles (surface angle of orientation/repose of pile sample after pouring from container) eroded more than soils with higher angles. Since measurements therein determined that the Ottawa sand repose angle ($\sim 25^\circ$) was smaller than that for WSMR ($\sim 35^\circ$), it follows that, to the first order, Ottawa sand scouring rates will be higher, as measured.

This finding, it should be noted, is in conflict with the expected variation of scouring rate (streamwise flux) with particle size as predicted by Bagnold (1941). His analysis suggests that, for suspension-type flows, Q will vary inversely with particle diameter. (For saltation flow Q is predicted to vary with diameter to the one-half power.)

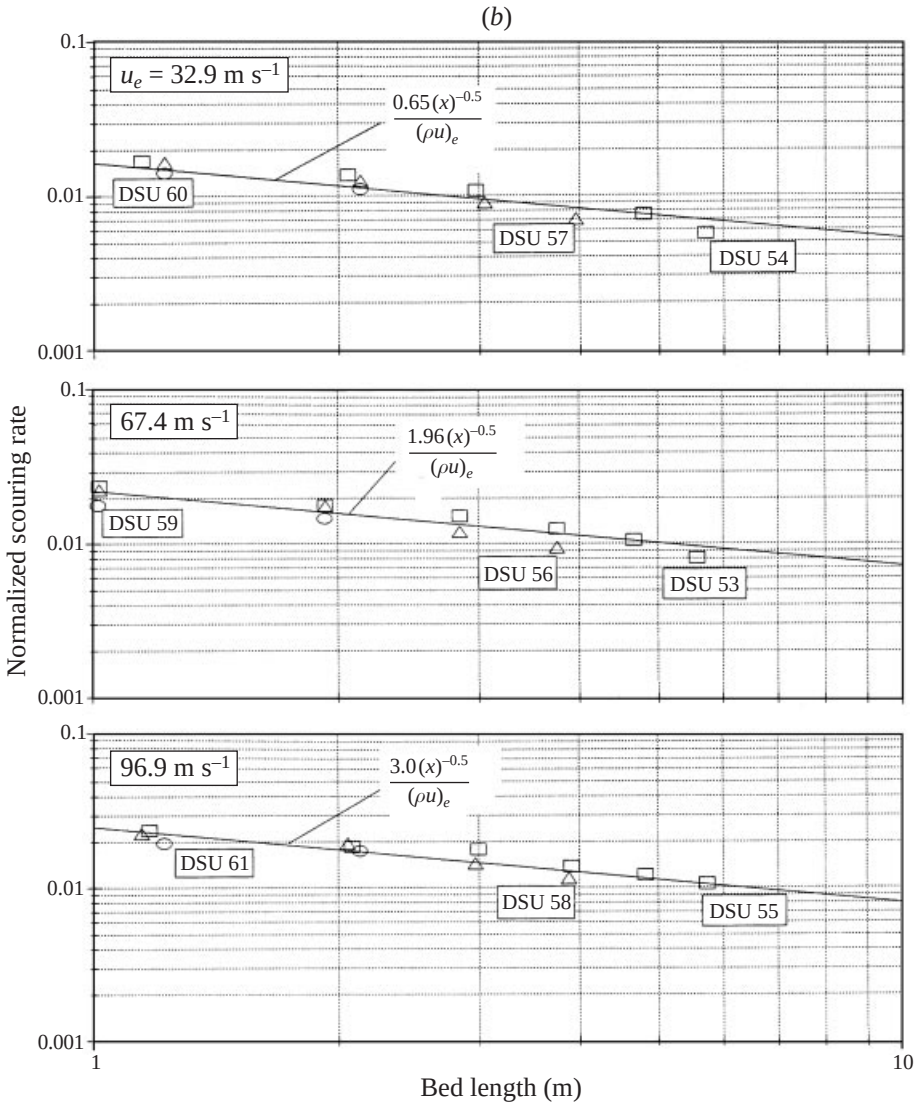

FIGURE 13. Variation of normalized scouring rate ($\overline{m}_s/(\rho u)_e$) with bed length for three boundary layer edge velocities (u_e): (*a*) WSMR and (*b*) Ottawa sand soil beds.

However, his suspension flow formulation is based on comparing the entrainment behaviour between monosized soil samples which do not incorporate the cohesive or frictional effects of natural soils. It is for this reason that the angle of repose has been considered herein as an approximate, albeit crude, measure of a soil's potential to erode. It represents a measurement approach by which soil samples can be empirically classified. Although the current results are encouraging, they are limited to one natural (WSMR) and one monosized (Ottawa sand) soil sample. Clearly, testing of additional soil materials is warranted to validate the present approach to characterizing a soil's scouring behaviour.

Further evidence of soil scouring dependence on velocity/Mach number is illustrated by the summary plot in figure 14(*b*) of streamwise soil flux data. Both profile

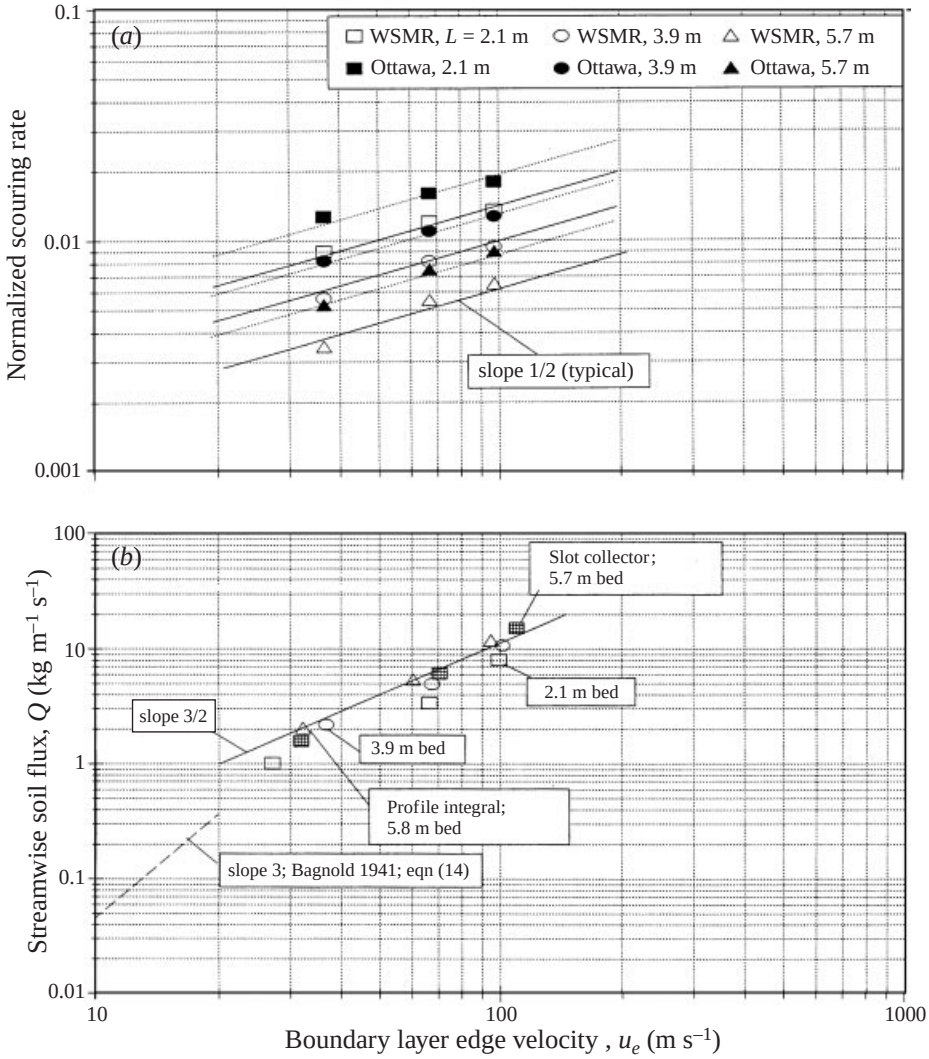

FIGURE 14. Variation of (*a*) normalized scouring rate ($\overline{m}_s/(\rho u)_e$) and (*b*) streamwise soil flux (Q) with boundary layer edge velocity (u_e) for three bed lengths.

integrated results (equation (9)) and Q data measured with a vertical slot collector (Bagnold 1941; Fryrear 1984 and Batt & Peabody 1999) are shown. Note the good agreement between the two measurement techniques. A variation of soil flux data with velocity/Mach number to the $\frac{3}{2}$-power is in evidence which is consistent with the observed dependence of $\overline{m}_s$ on velocity. The $\frac{3}{2}$-power velocity behaviour is also in agreement with the relationship for Q given by equation (10), the square-root dependence of bed length on velocity (figure 6) and the approximate similarity in the velocity and dust density profiles (figures 7 and 11). For example, note that

$$Q \sim u_e \delta_u \quad \text{(from equation (10))}$$

and for $\delta_u \sim u_e^{1/2} x^{1/2}$ (from figures 5 and 6)

$$Q \sim u_e^{3/2} x^{1/2} \quad \text{(as measured, figures 12 and 14}b\text{).}$$

In addition note also that

$$\overline{m}_s \equiv \mathrm{d}Q/\mathrm{d}x \quad \text{(equation (11))}$$
$$\sim u_e \mathrm{d}\delta/\mathrm{d}x \quad \text{(from equation (10) and flow similarity),}$$

giving

$$\overline{m}_s \sim u_e^{3/2} x^{-1/2} \quad \text{(again as measured, figures 13 and 14}a\text{).}$$

The observed sensitivity of Q and $\overline{m}_s$ to free-stream velocity is in contrast to soil loss data for comparable particle sizes for low-speed flows as measured by the data of Bagnold (1941), Chepil (1945), Owen (1964), Gillette & Passi (1988), Fletcher (1976) and Shao *et al.* (1993). For most low-speed flows a power-law dependence to the cube power of velocity is indicated. Note in figure 14(*b*), for example, the results of Bagnold (1941) based on his formula for rate of movement of natural sand of 250 μm particle diameter, namely

$$Q = 1.8\,(\rho_{air}/g)\,(u_f)^3. \tag{14}$$

Here, ρ_{air} refers to ambient air density and g is the gravitational constant. For the empirical curve shown in figure 14(*b*) a friction velocity ratio (u_e/u_f) of 17 has been assumed, consistent with the measurements of Bagnold (1941).

The indicated difference in power-law behaviour is considered an important distinction between the present high-speed results ($27 \leqslant u_e \leqslant 101\,\mathrm{m\,s^{-1}}$) and previous low-speed measurements ($u_e \leqslant 15\,\mathrm{m\,s^{-1}}$). Note that the cube-power dependence on velocity cited above for low-speed flows is associated with the saltation mechanism for particle motion based on the interplay between particle bombardment/collision and gravitational effects (Bagnold 1941; Owen 1964; Shao *et al.* 1993). As velocity increases, the boundary layer's turbulent eddy motion will have more control on the particle movement process (turbulent burst effects, eddy lift forces, etc., e.g. Cleaver & Yates 1973). At a sufficiently high velocity a transition takes place from a saltation-dominated process for particle motion to one associated with the complex problem of the high-speed multi-component turbulent boundary layer with mass addition. At the significantly increased mass loadings near the soil surface for these flow conditions fluid speeds decrease and consequently the rate of entrainment is reduced.

Note that for the current set of experiments, free-stream drag-to-weight ratios (D/W) for newly ejected particles are of the order of 100–1000. Here, the sphere drag relationship given by

$$D = 0.5\,C_D \rho_e u_e^2 A_p \tag{15}$$

has been used, with C_D referring to the particle drag coefficient (Schlichting 1955) and A_p the particle frontal area. Also for results herein, estimated free-stream particle Reynolds numbers,

$$\mathrm{Re} = \rho_e u_e D_p/\mu_e, \tag{16}$$

where μ_e corresponds to the boundary layer edge viscosity, are approximately 400–1200 and ratios of eddy velocity ($u_{eddy} \approx 0.1 u_e$; Hinze 1959) to particle terminal velocity ($u_{terminal} \approx 1\,\mathrm{m\,s^{-1}}$; Bagnold 1941) are $3 \leqslant u_{eddy}/u_{terminal} \leqslant 11$. These ranges in flow parameters, as well as relationships (6) and (7), further emphasize the suspension-flow nature of the current experiments.

Several investigators have addressed with detailed analyses the issue of dust entrainment by the high-speed turbulent boundary layer (e.g. Hartenbaum 1971; Mirels 1984; Denison & Hookham 1996). It is interesting to note that Hartenbaum (1971) and Mirels (1984) found that for conditions of the Hartenbaum measurements, which

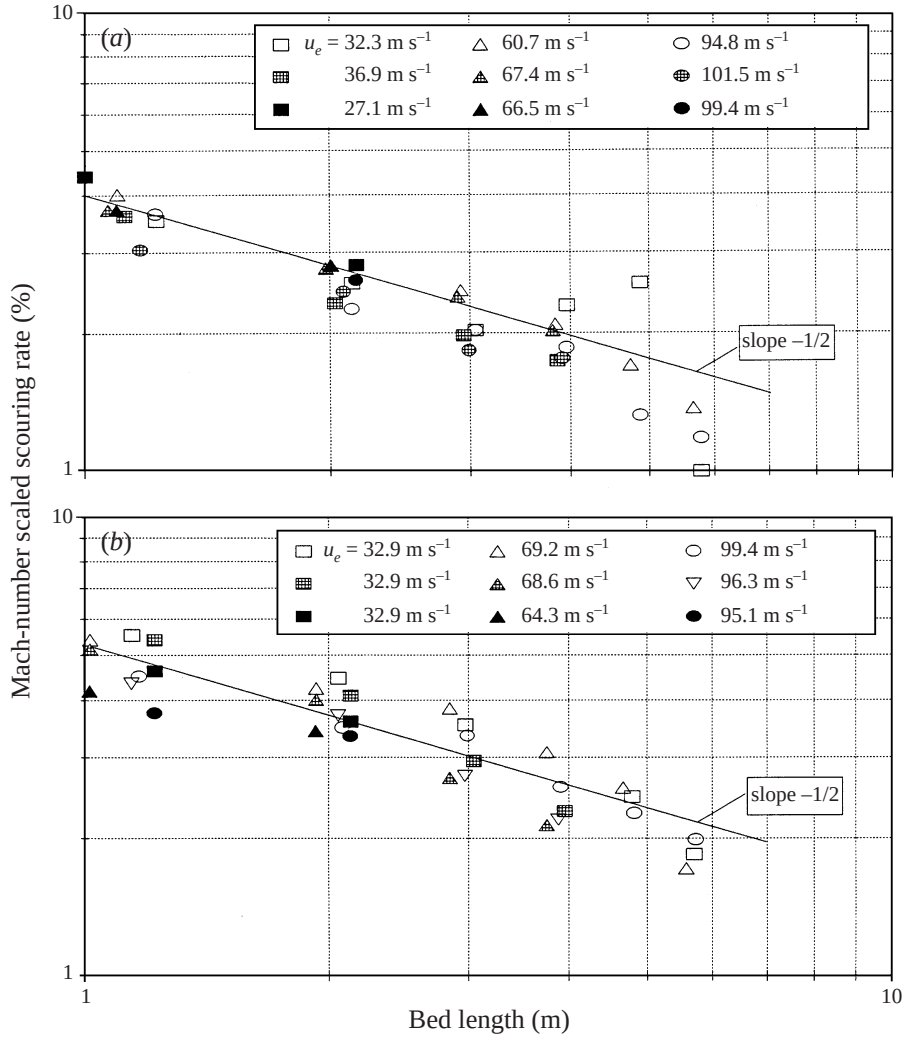

FIGURE 15. Variation of Mach-number-scaled (M) scouring rate ($[\overline{m}_s/(\rho u)_e]/M^{0.5}$) with bed length for (*a*) WSMR and (*b*) Ottawa sand soil beds for three boundary layer edge velocities (u_e).

are similar to the current experiments, streamwise flux data varied with velocity to a power law not only smaller than Bagnold's saltation result but even lower than the present data ($Q_{Hartenbaum} \sim u_e^{9/8} - u_e^{5/4}$).

A modest attempt has been made herein to provide a physical basis in support of the current measurements. Experiments as performed have addressed the issue of high-speed turbulent boundary layer flow with mass addition, in contrast to low-speed saltation-type flow. For example: results have been shown to correspond to the suspension regime for particle motion; the data agree favourably with flow similarity analyses for turbulent boundary layers; turbulent boundary layers with blowing behave in a similar manner; near-surface mass loadings are large and will tend to reduce dust layer velocities and soil scouring rates; and data consistency is well supported by independent measurements and other analyses and experimental results. A more detailed treatment of particle entrainment by the high-speed turbulent

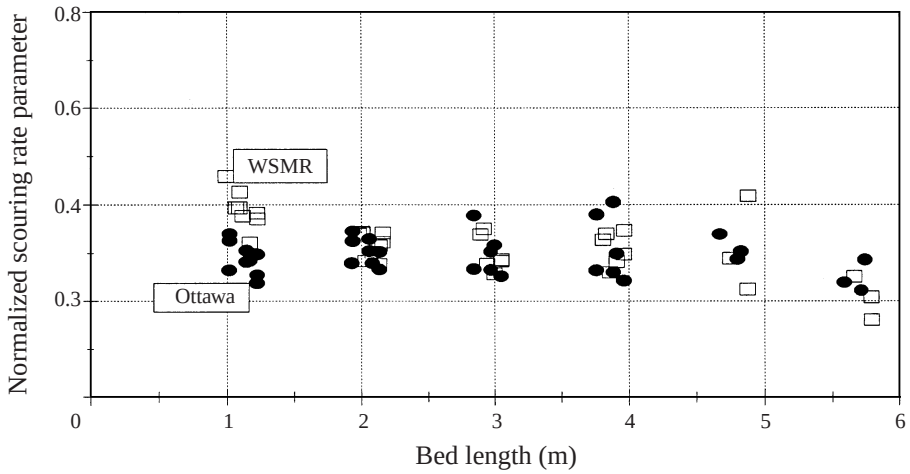

FIGURE 16. Variation of universal scouring rate parameter $(\overline{m}_s(\alpha/\alpha_{WSMR})/(\rho_e u_f)/M^{0.5})$ with bed length for WSMR (□) and Ottawa ● sand soil beds.

boundary layer, however, is still warranted. Such an effort is considered beyond the scope of the present study and attention herein has, instead, been directed more towards validating reduced results and demonstrating self-consistency between the independent measurements, with the hope that the overall data base will prove useful to those workers analytically treating this complex and important problem.

By use of Mach number (M_e) scaling, $\overline{m}_s \sim M_e^{3/2}$, an approximate collapsing of the scouring rate data base is achieved (figure 15), even though results still display sensitivity to bed length and soil type. An attempt to account for these letter effects has been made (figure 16) by first normalizing measured rates by the friction velocity mass flux ($\rho_e u_f$), instead of the edge flow mass flux ($\rho_e u_e$) thereby accommodating the bed length dependence, and then applying an approximate gain factor based on the ratio of soil-dependent repose angles (α). The resulting scaling factor is given by

$$\overline{m}_s(\alpha/\alpha_{WSMR})/(\rho_e u_f M_e^{1/2}) \approx 0.3 \pm 0.1. \tag{17}$$

It is interesting to note that this scaling procedure is similar to one suggested by various workers investigating the dusty boundary layer problem (e.g. Denison & Baum 1986; Gaj & Small 1991; Traci *et al.* 1987; Rosenblatt 1981). For comparison purposes, Traci *et al.* (1987) and Rosenblatt (1981) suggested constant values for $\overline{m}_s/(\rho_e u_f)$ of 0.33 and 0.4, respectively.

4. Conclusions

Experiments on entrainment of sand-sized particles in high-speed boundary layers have been conducted in a dust sweep-up wind tunnel at square-pulse flow speeds up to 101 m s^{-1} and for dust bed lengths up to 5.8 m. Results are obtained characterizing dusty boundary layer behaviour for both WSMR dust ($\overline{D}_{50} \approx 180\,\mu$m) and monosized Ottawa sand ($\overline{D}_{50} \approx 250\,\mu$m) soils. Measurements of local boundary layer velocities and dust densities were performed with traversing state-of-the-art diagnostics. Scouring rate data and streamwise soil flux as a function of bed length and free-stream velocity were determined.

4.1. *Velocity profiles*

Reduced boundary layer velocity data for both soil types tested behaved in an approximately self-similar manner and followed a power-law formulation given by

$$u/u_e = (y/\delta_u)^n.$$

Here, u_e corresponds to free-stream velocity, y represents elevation above the dust bed surface, δ_u is the velocity tangent-slope thickness in log-log coordinates and n is the power-law exponent. The WSMR data were found to scale well for a range in n values given by $n \approx 0.5 \pm 0.05$ whereas the Ottawa sand data were better represented by $n \approx 0.65 \pm 0.1$. Velocity thickness data varied with the square root of distance and velocity.

Dust velocity profiles also exhibit typical law-of-the-wall characteristics and correlate satisfactorily using a friction velocity ratio ($u_e/u_f = 15 \pm 3$). Friction velocities were found to increase linearly with edge velocity but decay with the inverse of the square root of bed length.

4.2. *Dust density profiles*

Dust loading factor profiles ($k = \rho_d/\rho_e$) for both soil types agree favourably with a curve fit formulation based on an inverse linear decay law given by

$$k = k_{1/2}[(y/\delta_d)^{-1} - 1].$$

As with the velocity data, a matching of a two-parameter fit at two data points satisfactorily determined a given profile result with $k_{1/2}$ corresponding to the loading factor value at the half-thickness point and δ_d to the dust loading factor thickness. Summarized thickness data illustrate that dust boundary layer edges ($\delta_d \sim x$) extend to higher elevations than corresponding velocity edges ($\delta_u \sim x^{1/2}$). This result demonstrates that particles reach free-stream elevations and is consistent with a less-than-unity turbulent Schmidt number ($Sc \approx 0.7$).

4.3. *Dust scouring rates*

Normalized scouring rates ($0.004 \leqslant \overline{m}_s/\rho_e u_e \leqslant 0.025$) determined from pre/post-test measurements of dust bed surface recession or mass loss compared favourably. Such rates were found to increase approximately as the $\frac{1}{2}$ power of free-stream velocity ($\overline{m}_s \sim u_e^{3/2}$) but decay as the inverse square root of dust bed length. Comparison of measured rates with independently derived rate results based on the rate of change of streamwise soil flux with distance was favourable. WSMR rates were always lower than corresponding Ottawa sand data, a result consistent with a lower repose angle for Ottawa sand ($\approx 25°$) than that for the WSMR soil ($\approx 35°$).

Soil loss rate (streamwise soil flux, $10 \leqslant Q \leqslant 150\,\mathrm{g\,cm^{-1}s^{-1}}$) as measured either by profile-integrated results or with a vertical slot collector (both measurements agree favourably), was found to increase as the $\frac{3}{2}$-power of edge velocity/Mach number. This high-speed result is in contrast with established data for comparable particle sizes for low-speed flows ($u \leqslant 15\,\mathrm{m\,s^{-1}}$; $Q \leqslant 1.5\,\mathrm{g\,cm^{-1}\,s^{-1}}$) where a power-law dependence to the cube power of velocity is indicated. The more modest sensitivity of soil flux to free-stream velocity for the current high-speed measurements may in part be explained as resulting from the dominating effects on particle motion of turbulent boundary layer phenomena and high near-surface mass loadings in contrast to low-speed flows where saltation processes are controlling.

Because friction velocities (u_f) decay approximately as the inverse square root

of distance, the observed decay behaviour in scouring rate ($\overline{m}_s$) with bed length is substantially reduced when lofting rates are normalized by a mass flux ($\rho_e u_f$) based on friction velocity rather than edge velocity. It was found also that rate dependence on soil type can be accounted for in an approximate manner by use of a soil-dependent gain factor based on a soil's repose angle (α). This correlation approach, when the data are also normalized by the square root of the boundary layer edge Mach number (M_e) to account for edge velocity dependence, corresponds to an approximately constant scouring rate value for both WSMR and Ottawa sand soil beds and for bed lengths up to 5.8 m in extent. This universal rate is given by

$$\overline{m}_s(\alpha/\alpha_{WSMR})/(\rho_e U_f M_e^{0.5}) \approx 0.3 \pm 0.1.$$

This work was sponsored by the Defense Special Weapons Agency under contract DNA 001-89-C-0079. The authors wish to thank Major D. P. Wade and Dr C. R. Gallaway, the technical monitors at the start and conclusion of the DSU program, respectively, for their direction, support and encouragement. Special thanks are also due to Drs A. Kuhl and M. Sanai, Professor T. Kubota and Ms K. Lode for their many valuable discussions and technical recommendations.

REFERENCES

Bagnold, R. A. 1941 *The Physics of Blown Sands and Desert Dunes*. Methyen and Co. Ltd. London.

Barthel, J. R. 1990 2D Hydrocode computations using a $K-\varepsilon$ turbulent model: Model description and test conditions. *Defense Nuclear Agency* DNA-TR-89-20.

Batt, R. G., Petach, M. P., Peabody II, S. A. & Batt, R. R. 1993 Experimental investigation of vegetation and dust sweep-up. *Defense Nuclear Agency* DNA-TR-92-53.

Batt, R. G. & Peabody II, S. A. 1995 Dust sweep-up experiments. Defense Nuclear Agency DNA-TR-94-117.

Batt, R. G. & Peabody II, S. A. 1999 Entrainment of fine sand particles from rough surfaces at high wind speeds. *Trans. ASAE* **42**, 1, 79.

Batt, R. G., Petach, M. P. & Peabody II, S. A. 1995 Development and application of stagnation pressure probe for dusty gas measurements. *Rev. Sci. Instrum.* **66**, 4356.

Chepil, W. S. 1945 Dynamics of wind erosion: III. The transport capacity of the wind. *Soil Sci.* **60**, 475.

Cleaver, J. W. & Yates, B. 1973 Mechanism of detachment of colloidal particles from a flat substrate in a turbulent flow. *J. Colloid Interface Sci.* **44**, 464.

Denison, M. R. & Baum, E. 1986 Non-ideal airblast subscale phenomenology experimentation program, Volume 1 – Boundary layer analysis. *Defense Nuclear Agency* DNA-TR-87-3-VI.

Denison, M. R. & Hookham, P. A. 1996 Modeling of dust entrainment by high-speed airflow. *AIAA J.* **34**, 1392.

Fletcher, B. 1976 The erosion of dust by an airflow. *J. Phys.* D: *Appl. Phys.* **9**, 913.

Fryrear, D. W. 1984 Soil ridges-clods and wind erosion. *Trans. ASAE* **27**, 445.

Gaj, R. A. & Small, R. D. 1991 Target area operating condition: Vol. 4, Dust lofting from natural surfaces. *Defense Nuclear Agency* DNA-TR-90-71.

Gillette, D. A. & Passi, R. 1988 Modeling dust emission caused by wind erosion. *J. Geophys. Res.* **93**, 14, 233.

Hartenbaum, B. 1971 Lofting of particulates by a high speed wind. *Defense Nuclear Agency* DNA 2737.

Hinze, J. O. 1959 *Turbulence*. McGraw-Hill.

Kuhl, A. L., Chien, K. Y., Ferguson, R. E., Collins, J. P., Glaz, H. M. & Collela, P. 1990 Simulation of a turbulent dusty boundary layer behind a shock. In *Current Topics in Shock Waves*, pp. 762–769. American Institute of Physics.

Mirels, H. 1984 Blowing model for turbulent boundary-layer dust ingestion. *AIAA J.* **22**, 1582.

Owen, P. R. 1964 Saltation of uniform grains in air. *J. Fluid Mech.* **20**, 225.

Rosenblatt, M. 1981 Introduction to nuclear dust/debris cloud formation. *Defense Nuclear Agency* DNA 5832T.

Schlichting, H. 1955 *Boundary Layer Theory*. Pergamon.

Shao, Y., Raupach, M. R. & Findlater, P. A. 1993 Effects of saltation bombardment on the entrainment of dust by wind. *J. Geophys. Res.* **98**, 12, 719.

Traci, R. M., Harris, T. B., Su, F. Y. & Phillips, G. T. 1987 Computation analysis of non-ideal airblast phenomenology. *Defense Nuclear Agency* DNA-TR-87-153.